17th World Conference on Earthquake Engineering, 17WCEE
Sendai, Japan - September 13th to 18th 2020

SEISMIC RESPONSE CHARACTERISTICS IN THE VALLEY PLAIN ALONG THE KANDA RIVER DUE TO THE DIFFERENCE IN EARTHQUAKE MOTION

D. Okukura[(1)], S. Yasuda[(2)], K. Ishikawa[(3)]

[(1)] *Graduate Student, Tokyo Denki University, 19rmg01@ms.dendai.ac.jp*
[(2)] *Professor Emeritus, Tokyo Denki University, yasuda@g.dendai.ac.jp*
[(3)] *Associate Professor, Tokyo Denki University, ishikawa@g.dendai.ac.jp*

Abstract

In the center of Tokyo, a valley plain exists with a dendritic shape, and structures and commercial facilities that are important to the country are concentrated within this plain. During the Great Kanto Earthquake in 1923, many buried pipes broke, and wooden houses collapsed along the valley plain. This level of damage is thought to be caused by amplification of seismic motion by the prevalence of soft organic soil and alluvial clay in the valley plain and the effects of the irregular formation of the alluvium based on the seismic response. The authors have carried out a two-dimensional (2D) earthquake response analysis using FLUSH, a software tool for conducting 2D finite element method (FEM) analyses of seismic responses, on a three-dimensional (3D) modeled section of the valley plain along the Kanda River that incorporated boring log. The input seismic motion was a seismic wave simulated for the Tokyo Bay coastal area whose predominant period was approximately 0.6 s to 0.8 s. In this study, also the seismic waves recorded at K-NET Shinjuku NS during the Great East Japan Earthquake were used to examine the effect of the frequency characteristics of the seismic ground motion on seismic response characteristics. The waveform in the seismic bedrock in earthquake engineering was computed from the ground surface using deconvolution. The predominant period of the input Shinjuku wave is approximately 1.0 s. The maximum ground surface velocity of the coastal wave, whose maximum input velocity to the bedrock was 51.58 cm/s, ranged from approximately 80–90 cm/s in the plateau and from approximately 90–100 cm/s in the peat layer and the alluvial clay layer inside the valley plain. The maximum ground surface velocity of the Shinjuku wave, whose maximum input velocity to the bedrock was 47.05 cm/s, ranged from approximately 90–100 cm/s at the plateau and from approximately 100–120 cm/s inside the valley plain. These results show that the ground in the valley plain tends to amplify the velocity response more than other ground, such as plateau. Moreover, the analysis reveals that the velocity response to long-period seismic waves in the valley plain along the Kanda River is amplified inside the lowlands, which occurs because the natural period of the ground inside the valley floor is close to the predominant period of the Shinjuku wave, and the ground resonates. In other words, the frequency characteristic of the seismic wave affects the seismic response of the valley plain. In addition, when the relationship between the alluvial clay layer thickness and the maximum surface velocity was examined, it was found that the maximum surface velocity increased as the alluvial clay layer thickness increased. Therefore, we conclude that the alluvial clay layer thickness affects the ground surface maximum velocity.

Keywords: valley plain, seismic response analysis, frequency characteristics

1. Introduction

A dendritic-shaped valley plain exists at the center of Tokyo. It is home to the country's major structures and commercial facilities. Owing to the Great Kanto Earthquake in 1923, buried pipes were damaged and wooden houses collapsed along the valley plain [1]. Such damage is believed to be caused by the amplification of seismic motion due to the prevalence of soft organic soil and alluvial clay in the valley plain and by the effects of the irregular formation of the alluvium resulting from the seismic response [1]. Owing to the seismic response characteristics of the surface layer of soft ground and its irregular base, it is feared that earthquake damage from tremors will occur at Tokyo's lowland in the event of a Tokyo inland earthquake, which is expected to occur in the future, or a large earthquake equivalent to the Great Kanto Earthquake in 1923. Therefore, it is vital to understand the structure of the low-lying ground in Tokyo and the impact of its shape on the seismic response of the surface layer to develop measures for ground disaster prevention. In this study, research on these issues was conducted in the valley plain along the Kanda River in central Tokyo to evaluate the seismic response characteristics of the shape of the irregular valley plain of Tokyo's lowland. Specifically, the following actions were carried out:

(1) The valley plain was modeled according to the 3D model reported by Kimura et al. [2].
(2) A 2D cross-section based on a boring log and a 3D model were created; the initial stress analysis in the ground models was performed.
(3) A seismic response analysis was conducted to calculate the acceleration, velocity, displacement, and horizontal strain at the time of the earthquake.
(4) A 1D seismic response analysis was conducted to examine the impact of seismic response by the irregular base of alluvium.

The following analysis programs were used in this study:

- Initial stress analysis: 2D Finite Element Method (FEM) static stress analysis ALID/Win Ver. 5.0
- Seismic response analysis: 2D FEM dynamic response analysis Advanced FLUSH/Win

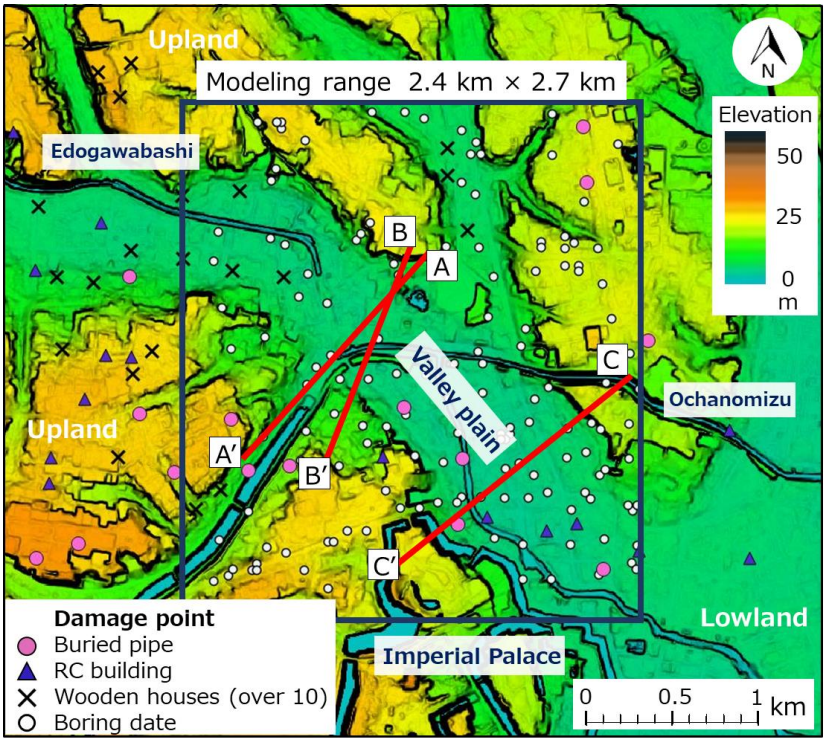

Fig. 1: Locations of the examined sidelines, locations of damage caused by the Great Kanto Earthquake in 1923, and locations of boring log.

2. Seismic response characteristics on irregular base in Tokyo lowland

2.1 Characteristics of the valley plain along the Kanda River and analysis cross-section

Fig. 1 depicts the digital elevation map of the area between Edogawabashi and Ochanomizu that contains the locations of cross-sections (red line) and the sites damaged by the Great Kanto Earthquake in 1923 [3]. The area from Edogawabashi to the lower Kanda River is characterized by the deep burial of soft alluvium at the bottom of the valley plain, which is carved by the recession of the sea in the low reference period of the glacial period. The shape of the valley is asymmetric with a steep north and a gentle south slope. The shape of the valley is known to differ according to the location [4].

As shown in Fig. 1, the analysis cross-section of the analysis was defined as follows:
Cross-section A-A': Cross-section in which peat is found to be buried from the existing boring log [5]
Cross-section B-B': Cross-section B-B' adjacent to the A-A' cross-section with little buried peat.
Cross-section C-C': Cross-section of the downstream area of the valley plain with thick deposition of alluvial cohesive.

2.2 Creation of 3D model

The 3D model was created using a program from the National Research Institute for Earth Science and Disaster Resilience. The method proposed by Kimura et al. [2] was followed. The 3D model was set at 100-m intervals, and 3D spatial interpolation was conducted on the soil. The SPT *N*-value resulting from the existing boring log in the modeling range is highlighted by a blue frame in Fig. 1. According to the aforementioned method, the reference radius of the boring log was set at 1000 m. The area was divided into two parts based on the north. The interpolation was calculated by a minimum of 1 point from each quadrant, and the inverse-distance weighting method was conducted by a maximum of 5 points. The weight coefficient was set to 2. The boundary conditions for the construction of the 3D model also provided the basal boundary of the alluvium and the surface elevation boundary. The basal boundary of the alluvium was prepared using boring log from information on the basal surface depth of the alluvial layer determined according to a geological interpretation of the alluvial and flood lamination. The ground-surface elevation information was obtained from a 5-m digital elevation model from the Geospatial Information Authority of Japan. The 3D model is characterized by the ability to represent the geological structure without requiring geological interpretation because the grid without ground information can be interpolated with the soil and the *N*-value by the inverse-distance weighting method.

2.3 Method for creating analysis cross-section

Ground modeling requires varied information. The interpretation and use of the data are judged to be satisfactory. In this case, the ground model was created using the existing boring log published by Metropolitan Tokyo based on the boring log [5]. Geological interpretations were added based on the Tokyo Metropolitan Comprehensive Geographical Map [6]. In contrast, the ground model was created by spatial interpolation using a 3D model. Fig. 2 shows a ground model diagram based on ground information in the A-A', B-B', and C-C' cross-sections. A general ground model diagram using a boring log is shown in Fig. 2 on the left, whereas one with space interpolation using a 3D model is shown on the right. Note that A-A', B-B', and C-C' cross-sections are shown in the upper part in Fig. 2. From the 2D cross-sectional view of each section, the bottom of the valley is filled with high organic matter and alluvial clay, forming an asymmetric valley with a river terrace on both sides. In addition, when the boring log and 3D model are used, there are differences in the thickness of the peat layer and the shape of the basal surface of the offshore lamination.

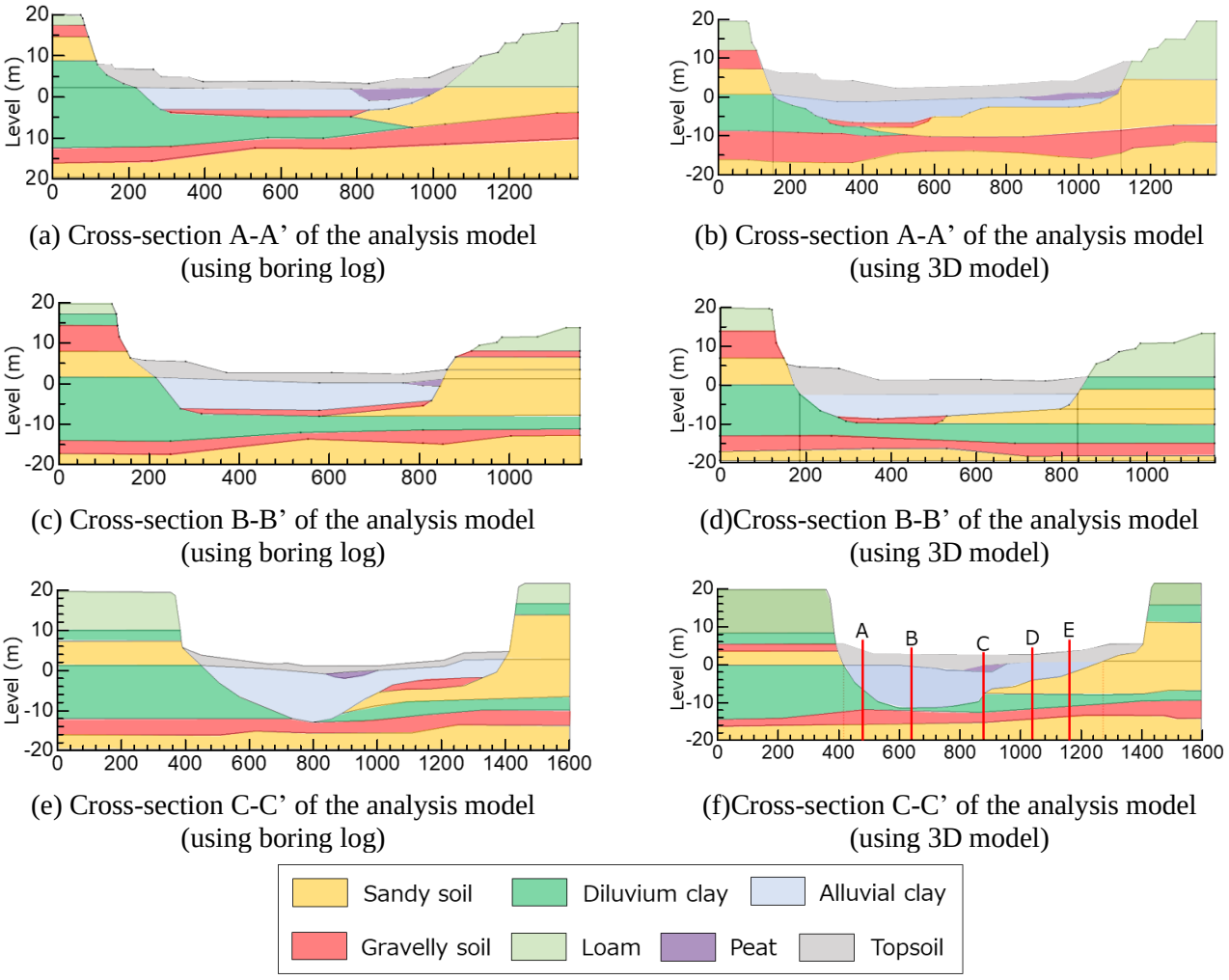

(a) Cross-section A-A' of the analysis model (using boring log)

(b) Cross-section A-A' of the analysis model (using 3D model)

(c) Cross-section B-B' of the analysis model (using boring log)

(d)Cross-section B-B' of the analysis model (using 3D model)

(e) Cross-section C-C' of the analysis model (using boring log)

(f)Cross-section C-C' of the analysis model (using 3D model)

Fig. 2: Cross sections of the analysis models.

2.4 Terms and conditions of the analysis

Fig. 3 shows that the input seismic motion was a wave simulated for the Tokyo Bay coastal area (referred to as Case 1). The seismic waves recorded at K-NET Shinjuku NS during the Great East Japan Earthquake (Case 2) were also used to examine the effect of the frequency characteristics of the seismic ground motion on seismic response characteristics. The waveform in the seismic bedrock in earthquake engineering (assuming a shear wave velocity of V_S = 350 m/s) was computed from the ground surface using deconvolution, and the waveform amplitude was adjusted to the acceleration for Case 1. We considered a maximum acceleration of 310.6 cm/s^2 and a maximum velocity of 47.1 cm/s). In the deconvolution, the dynamic deformation properties were based on the equation proposed by Yasuda and Yamaguchi [7]. The shear wave propagation velocity V_s and the wet density ρ_t were based on the soil data of K-NET Shinjuku published by the National Research Institute for Earth Science and Disaster Resilience [8]. The acceleration and velocity response spectra of seismic waves produced by using the acceleration waveforms in Figs. 3 and 4 are in Fig. 5. In Case 1, short-period components predominate between 0.2 s and 1.0 s, while in Case 2, the velocity response of long-period components ranging from 1.0 s to 1.5 s predominates, demonstrating the difference in the frequency characteristics of both seismic motions.

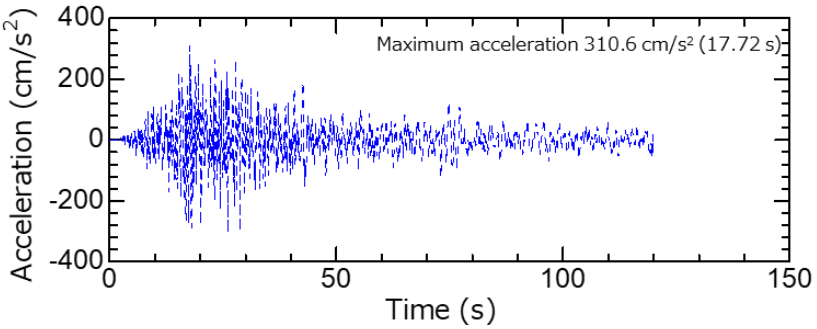

Fig. 3: Time history of input earthquake motion (Case 1).

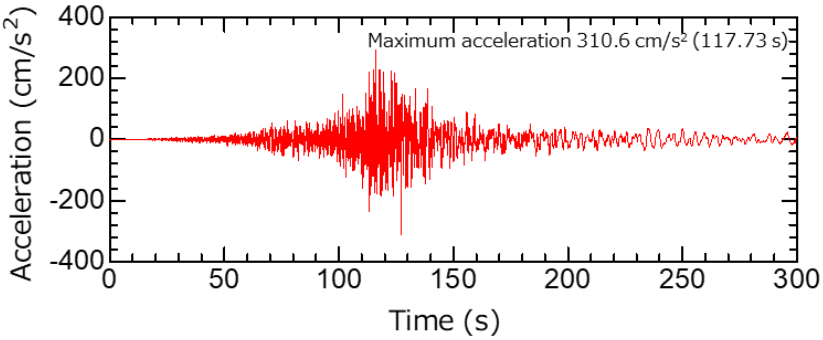

Fig. 4: Time history of input earthquake motion (Case 2).

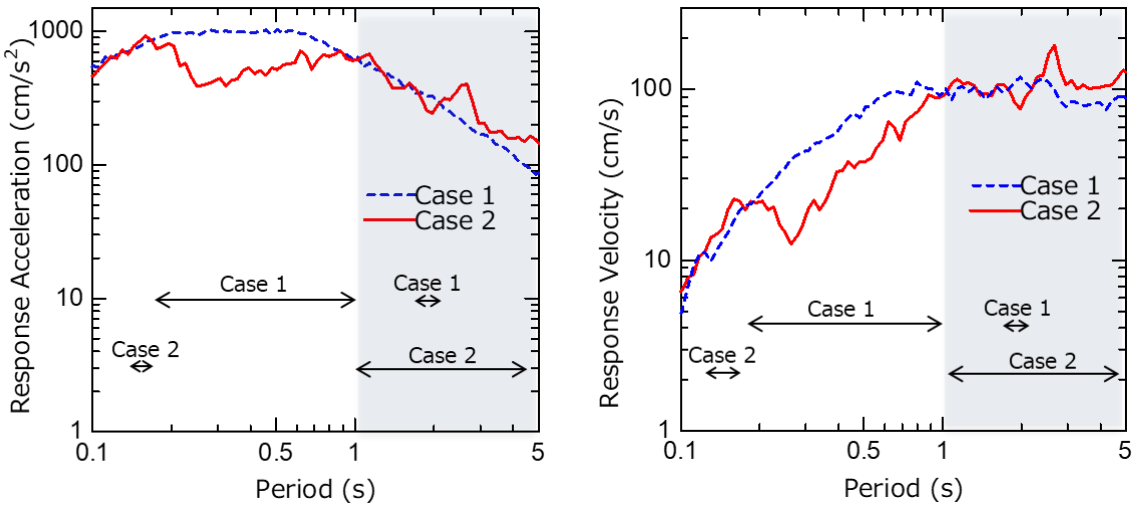

Fig. 5: Response spectrum in Case 1 and Case 2 (damping ratio: 5 %).

2.5 Physical properties of the soil used in analysis

Table 1 lists each physical property value in the C-C' section. SPT *N* values were obtained from ground information and averaged within the same soil classification.

(1) Soil constants used in the initial stress analysis

• Shear modulus *G* (kN/m ^{2}): it was obtained from-the-following requests:

$$E = 2800 \times N \quad (1)$$

$$G = E / 2 \times (1 + \nu) \quad (2)$$

N : N-value by SPT, ν : Poisson's ratio

The unit weight was set according to Metropolitan Tokyo [9].

• Stress-dependent coefficient *K* (kN/m ^{2}),

$$K = E / (\sigma_m / P_a)\, n \quad (3)$$

The Janbu expression parameter n was set to 0.5 for sandy soil and 1.0 for cohesive soil. The mean principal stress, based on the effective stress at the center depth of each layer was set as $K_0 = 0.5$.

(2) Soil properties used in the seismic response analysis

• Shear modulus at small strain G_0 (kN/m^2): it was calculated through the following equations:

Sandy soil $V_s = 80 \times N^{1/3}$ (4)

Cohesive soil $V_s = 100 \times N^{1/3}$ (5)

$$G_0 = \rho \times V_s^2 \quad (6)$$

For peats, G_0 was set at 2200 kN/m ^{2} using the result of a dynamic deformation property test [10] based on previous studies.

The mean diameter D_{50} (mm) was set from the Tokyo Metropolitan Liquefaction Forecast [9].

• The relationship between the shear strain, γ, the dynamic shear modulus ratio, G/G_0, and the damping ratio, *h*, for each layer water was set by using the estimation formula proposed by Yasuda and Yamaguchi (1985).

Table 1: Physical properties of the respective layers used for the analysis.

Layer	Soil property	γ (kN/m^3)	D_{50} (mm)	*N value*	*Vs* (m/s)	*E* (kN/m^2)	*G* (kN/m^2)	G_0 (kN/m^2)
Lm1	Loam	11.6	0.013	3.75	155	10500	3938	28541
Lm2	Loam	11.6	0.013	3.33	149	9324	3497	26368
Ho(g)	Coarse sand	17.5	0.365	45.7	286	127960	47997	145935
Ho(s)	Medium sand	17.1	0.26	42.5	279	119000	44636	135863
To1(s)	Medium sand	19.1	0.26	30.4	250	85120	31928	121374
To(c)	Silt	15.9	0.013	9.4	211	26320	9872	72190
F	Topsoil	11.6	0.013	6.3	184	17556	6585	40207
P	Peat	12.9	0.014	2	126	5600	2101	2200
Ac	Clay	15.4	0.011	1.11	104	3108	1166	16829
Ag	Coarse sand	19.5	0.365	20	217	56000	21005	93734
Tog	Coarse sand	19.5	0.365	50	295	140000	52513	172660
To2(s)	Medium sand	19.1	0.26	50	295	140000	52513	169118

3. Results of 2D seismic response analysis

3.1 Discussion on the effect of alluvial cohesive soil on seismic response characteristics

Fig. 6 shows the results of the analysis of the A-A' section, and Fig. 7 shows the results of the analysis of the B-B' section. These analyses were conducted for Case 1. Figs. 6 and 7 (a) to (d) depict the maximum acceleration distribution, maximum velocity distribution, maximum displacement distribution, and maximum horizontal strain distribution on the ground surface from the top. The results of the analysis on the ground model created solely from the boring log is shown on the left charts in these figures, whereas those resulting from spatial interpolation using the 3D model are shown on the right. The bottom of the valley plain of the A-A' section is filled with alluvium to form an asymmetric valley having a width of approximately 1000 m. On both sides of the valley, a fluvial terrace is formed. On the upper part of the valley plain, an alluvial clay is deposited, 6 m on the north side and 3 m on the south side, and the peat is approximately 2 m thick. The valley plain of the cross-section B-B' has an asymmetric valley; however, the valley plain has a width of approximately 700 m and is narrower than the cross-section A-A', and no peat is buried. As shown in the left charts of Figs. 6 (a), (b), and (c), the maximum acceleration was 577 cm/s^2 on the peat layer, approximately 500 cm/s^2 on the sloped terrace border, and approximately 550 cm/s^2 on the slope of plateau. In addition, the maximum horizontal displacement tended to amplify to approximately 10 cm on the peat layer. The maximum horizontal strain was approximately 0.15 % on the peat layer. In addition, as shown in the right charts of Figs. 6 (a), (b), and (c), the maximum acceleration was 683 cm/s^2 on the peat layer, approximately 400 cm/s^2 on the sloping terrace border of the base, and approximately 500 cm/s^2 on the plateau shoulder. In particular, the acceleration response in the upper layer of the peat layer is noticeable. In addition, the maximum horizontal displacement tended to be amplified by approximately 5 cm on the peat layer compared with other layers. Maximum horizontal strain occurred at the boundary of the plateau and the shoulder of the plateau with peats and a sloping base; however, the magnitude of the strain was only approximately 0.05 % in both compression and tension.

As shown in Figs. 7 (a) to (d), no significant seismic response occurred in the B-B' section. Based on these results, the presence or absence of peat and the geometry of the underlayer below the soft layer are believed to affect the difference in earthquake response irrespective of the method for preparing the ground model. The acceleration response of the upper organic soil layer and the shoulder of the plateau in the A-A' section is comparatively consistent with the damage caused by the Great Kanto Earthquake in 1923 shown in Fig. 1.

3.2 Effect of input seismic motion

Figs. 8 and 9 show the results of 2D seismic response analysis using the boring log and the 3D model, respectively. In these figures, the results of the analysis in Case 1 are shown in the left charts whereas the results of the analysis in Case 2 are shown in the right charts. Maximum acceleration distribution, maximum velocity distribution, maximum displacement distribution, and maximum horizontal strain of the ground surface are shown from the top of each figure. Only the results of the analysis of the C-C' section, in which peat is buried and soft alluvial clay is deposited at the thickest level, are presented in this paper. A comparison of the analysis results obtained in Case 1 and Case 2 shows no significant difference in the acceleration response; however, there is a difference in the velocity response. Note from Fig. 8 that the maximum surface velocity in Case 1 when using the boring log was in the range 80‑90 cm/s in the plateau and 90‑110 cm/s in the upper organic soil layer and the alluvial clay layer in the lower ground. The maximum surface velocity in Case 2 ranged from 100‑110 cm/s in the plateau and 110‑120 cm/s in the hilly organic soil layer and the alluvial clay layer. Note also from Fig. 9 that the maximum surface velocity in Case 1 using the 3D model was in the range 90‑100 cm/s at the plateau and 100‑110 cm/s above the peat layer inside the lower ground and the alluvial clay layer. The maximum surface velocity in Case 2 was in the range 100‑110 cm/s on the plateau, and the velocity response was significantly amplified in the peat layer inside the valley and in the alluvial clay layer, resulting in a velocity response in the range 100‑120 cm/s. In

addition, the maximum horizontal displacement response exhibited similar trends. According to these results, the velocity response of long-period seismic waves in the valley plain along the Kanda River tended to be amplified in the valley plain. This is probably because the predominant period of the seismic wave in Case 2 and the intrinsic period inside the valley plain resonated near each other. Although not shown here, the velocity response tended to be significantly amplified at the bottom of the valley even in the A-A' and B-B' cross-sections.

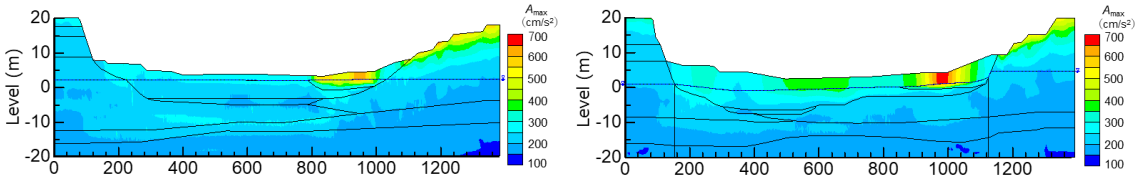

(a) Maximum acceleration distribution (left: using boring log, right: using 3D model)

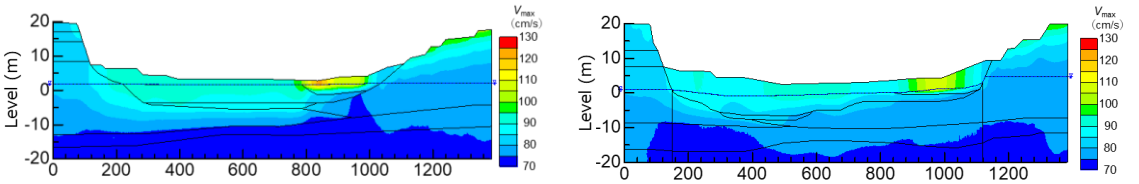

(b) Maximum velocity distribution (left: using boring log, right: using 3D model)

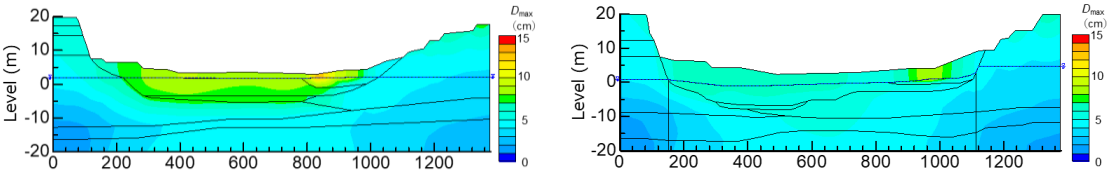

(c)Maximum displacement distribution (left: using boring log, right: using 3D model)

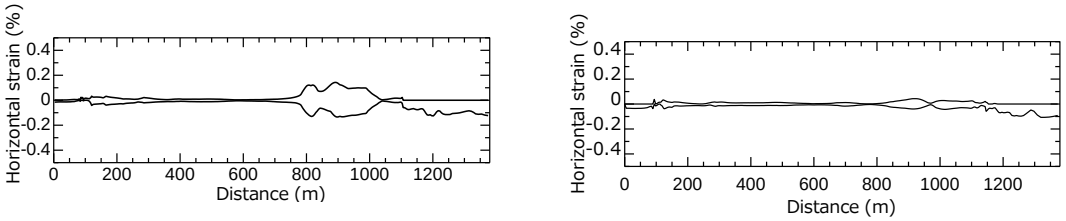

(d) Maximum horizontal strain distribution (left: using boring log, right: using 3D model)

Fig. 6: Cross-section A-A' of the analysis results.

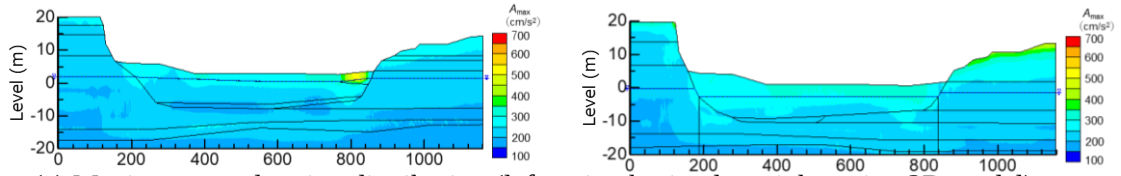

(a) Maximum acceleration distribution (left: using boring log, right: using 3D model)

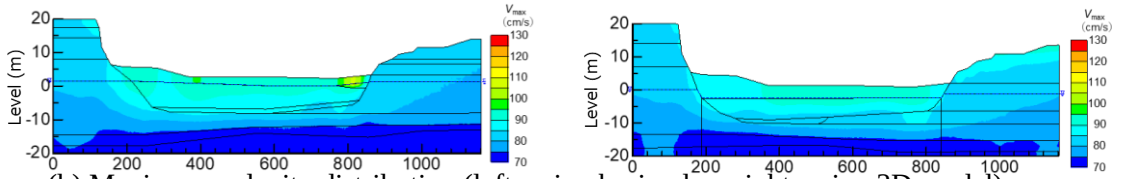

(b) Maximum velocity distribution (left: using boring log, right: using 3D model)

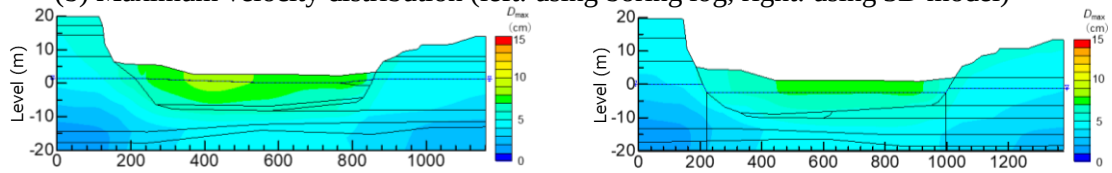

(c) Maximum displacement distribution (left: using boring log, right: using 3D model)

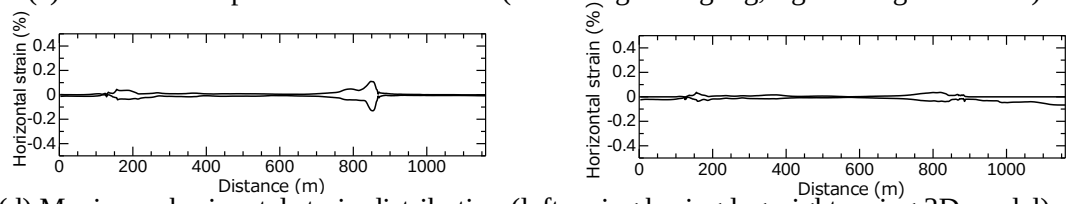

(d) Maximum horizontal strain distribution (left: using boring log, right: using 3D model)

Fig. 7: Cross-section B-B' of the analysis results.

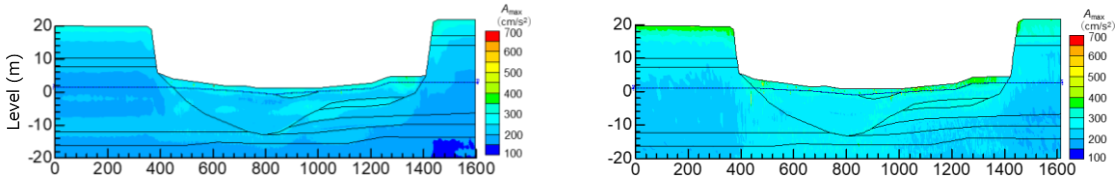

(a) Maximum acceleration distribution (left: Case 1, right: Case 2)

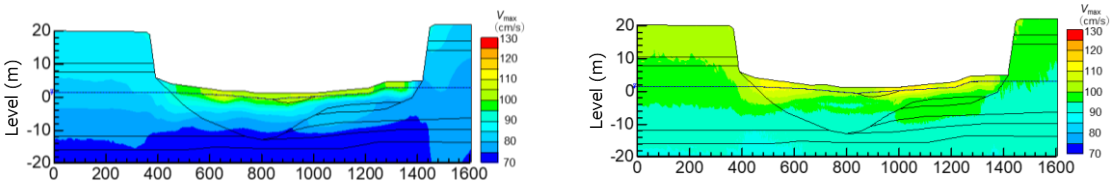

(b) Maximum velocity distribution (left: Case 1, right: Case 2)

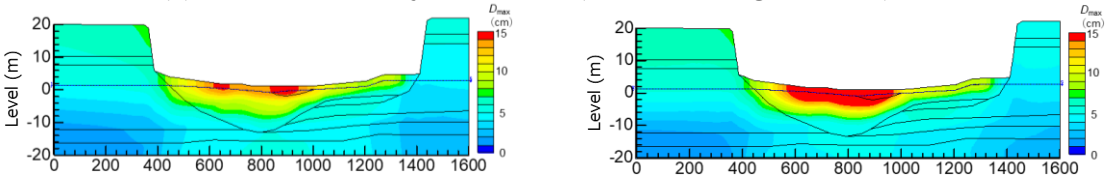

(c) Maximum displacement distribution (left: Case 1, right: Case 2)

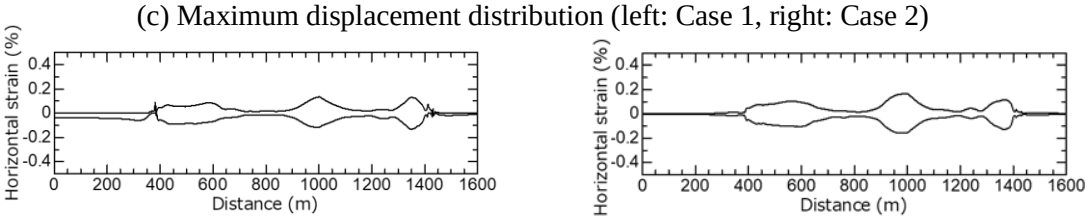

(d) Maximum horizontal strain distribution (left: Case 1, right: Case 2)

Fig. 8: Cross-section C-C' using boring log of the analysis results.

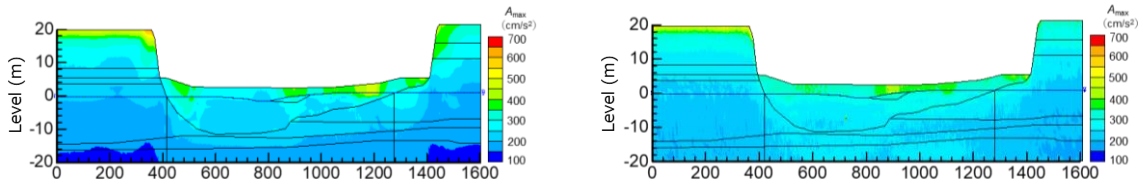

(a) Maximum acceleration distribution (left: Case 1, right: Case 2)

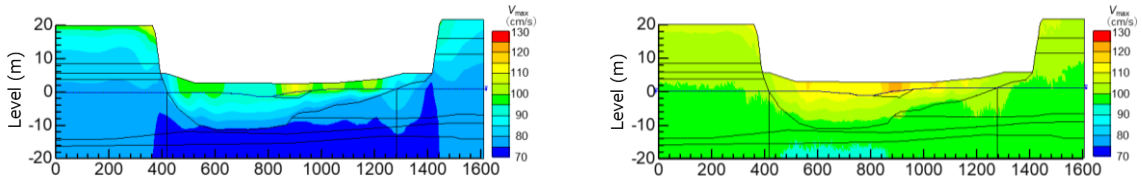

(b) Maximum velocity distribution (left: Case 1, right: Case 2)

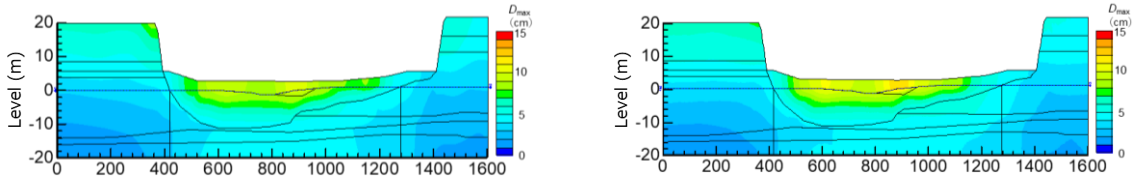

(c) Maximum displacement distribution (left: Case 1, right: Case 2)

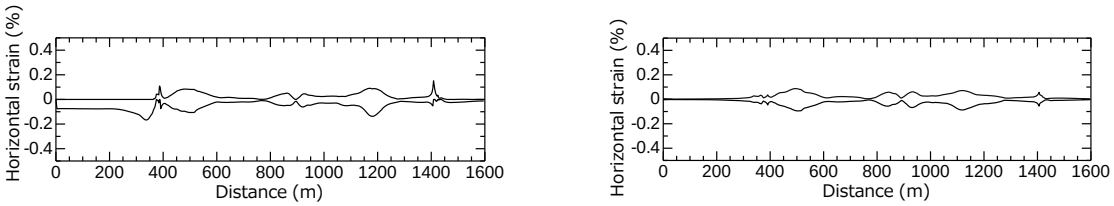

(d) Maximum horizontal strain distribution (left: Case 1, right: Case 2)

Fig. 9: Cross-section C-C' using 3D model of the analysis results.

3.3 Relationship of the maximum velocity response by the 1D seismic response analysis and the 2D seismic response analysis

1D cross-sections based on a 3D model were created at the focal point in the cross-section C-C'("A"-"E" in Fig. 2 (f)), and seismic response analyses were conducted using a 2D FEM dynamic response analysis Advanced FLUSH/Win. Terms and conditions of the analysis were the same as in the previous chapter.

Figures 10 shows the relationship between the maximum velocity response from the 1D seismic response analyses and the 2D seismic response analyses at the focal point in the cross-section C-C'("A"-"E" in Fig. 2 (f)) for each seismic wave. It was confirmed the maximum velocity response from the 2D seismic response analyses slightly exceeded the maximum velocity response from the 1D seismic response analyses, but the maximum velocity response from the 2D seismic response analysis at the center of the valley plain with the thickest alluvial layer was remarkable. In this point, it can be said that the effect of seismic response by the irregular base of alluvium is big. Therefore, the factors affecting the maximum velocity response vary from site to site even in the same valley plain.

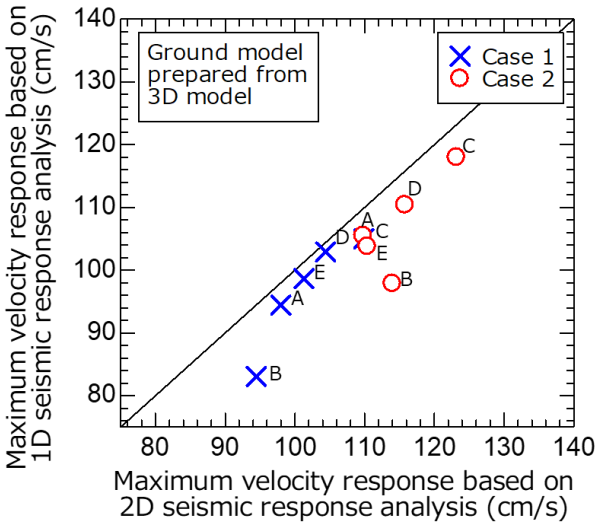

Fig. 10: Cross-section C-C' using 3D model of the relationship between the maximum velocity response from the 1D seismic response analysis and that from the 2D seismic response analysis.

4. Conclusion

A 2D seismic response analysis was conducted in the valley plain along the Kanda River for two seismic motions using two models with separate creation methods. As a result, the velocity response was amplified in the peat and alluvial clay layer inside the valley plain, irrespective of the method employed for the ground model. The long-period seismic waves also exhibited a tendency to amplify the velocity response within the valley plain. Furthermore, it was confirmed that the maximum velocity response from the 2D seismic response analyses were comparable to the maximum velocity response from the 1D seismic response analyses in both cases, but the maximum velocity by the 2D seismic response analysis near at the upper portion of the incline in the valley plain was remarkable. In this point, it can be said that the effect of seismic response by the irregular base of alluvium is big. Therefore, the factors affecting the maximum velocity response vary from site to site even in the same valley plain.

5. References

[1] Yasuda S, Watanabe H (2010): Study on the seismic response at the valley plains in Tokyo based on respresentative soil profile models. *13th Japan Earthquake Engineering Symposium*, 2019-2026, Japan. (in Japanese)

[2] Kimura K, Hanashima Y, Yamamoto K, Ishihara Y, Oji S, Wada R, Ooi M (2016): Methodology and applicability of 3D grid modelling based on borehole database for urban subsurface grounds. *51st Japan National Conference on Geotechnical Engineering*, 287-288, Japan (in Japanese)

[3] Yasuda S, Yoshikawa Y, Ushijima K (1993): Damage during an earthquake and soil profiles at valley plains in Tokyo, *Proc. of the 48th Japan National Conf. on Civil Engineering*, Part 3, 422-423. (in Japanese)

[4] Kubo S (1988): Some Geomorphological Features of Kanda River Valley around the Waseda University, Tokyo. *The scientific researches Vol.XXXVII issued annually by the school of education, Waseda university*, 57-73. (in Japanese).

[5] Metropolitan Tokyo HP(2018): The ground of Tokyo,

http://www.kensetsu.metro.tokyo.jp/jigyo/tech/start/03-jyouhou/geo-web/00-index.html

[6] The Inst. of Civil Engineering of The Tokyo Metropolitan Government (1977): Tokyo total subgrade map (I), 10-15. (in Japanese).

[7] Yasuda S, Yamaguchi I (1985): Dynamic soil properties of undisturbed samples, *Proc of the 20th Japan National Conf. on SMFE*, 539-542 (in Japanese)

[8] National Research Institute for Earth Science and Disaster Resilience HP:
http://www.kyoshin.bosai.go.jp/kyoshin/db/index.html?all

[9] Metropolitan Tokyo (2012): http://doboku.metro.tokyo.jp/start/03-jyouhou/ekijyouka/pdf/00_zenbun__.pdf

[10] Yasuda S, Aizu K, Fujita Y, Tochio T, Naoi K, Matsumoto S (2010): Dynamic shear modulus of the peat deposited in the valley plain in Tokyo. *45th Japan National Conference on Geotechnical Engineering*, 737-738, Japan (in Japanese)

